Tellus SERIES A DYANAMIC METEOROLOGY AND OCEANOGRAPHY
PUBLISHED BY THE INTERNATIONAL METEOROLOGICAL INSTITUTE IN STOCKHOLM

Three-dimensional potential vorticity structures for extreme precipitation events on the convective scale

By ANNETTE MÜLLER*, BENJAMIN NIEDRICH, and PETER NÉVIR, *Institute for Meteorology, Freie Universität Berlin, Berlin, Germany*

(Manuscript Received 14 April 2020; in final form 13 August 2020)

ABSTRACT

Three-dimensional potential vorticity (PV) structures on the convective scale during extreme precipitation events are investigated. Using the high resolution COSMO-REA2 data set, 3D composites of the PV, with and without Coriolis parameter and related variables, are evaluated for different classes of precipitation intensity. The development of a significant horizontal dipole structure in the immediate vicinity of the precipitation maximum and the updraft can be explained by the twisting term in the vorticity equation. This is because the vorticity equation is proportional to the PV equation for strong convective processes. This theoretical is important on the convective scale without the consideration of the Coriolis effect, which is a typical characteristic on the synoptic scale. In accordance to previous studies, the horizontal PV dipole is statistically confirmed by 3D composites of the PV and corresponding variables. We show that the dipole structures are especially distinct for the relative PV without Coriolis parameter and the relative vorticity. On the convective scale, the thermodynamical sources and sinks of the potential vorticity indicate the diabatic processes that are related to conservative vortex dynamics via the proportionality of the diabatic heating and the vertical velocity. This work confirms that the PV equation is an important tool in atmospheric dynamics that unifies the thermodynamical processes as well as the dynamical processes into one scalar.

Keywords: potential vorticity, twisting term, vorticity equation, extreme precipitation

1. Introduction

The potential vorticity is an important quantity in atmospheric dynamics that unifies the thermodynamical processes as well as the dynamical processes into one scalar. It was first derived by Ertel (1942a). Under adiabatic and inviscid conditions, the potential vorticity, short PV, is an individually conserved quantity for every Lagrangian particle. This conservation property of the PV is used on the synoptic scale in order to understand the evolution of the large scale high- and low pressure areas in the midlatitude, known as PV thinking (Hoskins et al., 2007). Moreover, Hoskins et al. (2007) analyze in detail the invertibility and individual conservation of the PV on the synoptic scale. Under quasi-balanced atmospheric conditions this enables the determination of the corresponding wind field, temperature and density from the PV. Furthermore, Davis (1992) compares different methods of PV inversions analyzing the inversion of individual portions of the potential vorticity field. Haynes and McIntyre (1987) underline the conservation of the PV by showing that 'The PV can neither be created or destroyed, within a layer bounded by two isentropic surfaces'.

Especially on the meso- and synoptic scale the PV has been used to study atmospheric processes and phenomena. Using the semi-geostrophic theory, Thorpe and Emanuel (1985) analyze the meso-scale frontal structure, showing that the PV is characterized by sources and sinks. Raymond and Jiang (1990) show a vertical dipole of PV anomalies on the meso-scale, which is produced by a region of convection and the associated changes in the temperature and wind structure. Based on linearized models with simple boundary conditions Persson (1995) shows the relation of PV dipoles to fronts using numerical simulations; Plant et al. (2003) use upper-level PV anomalies to study extratropical cyclones and Viúdez (2010) analyze the vertical split of vortices numerically considering the f-plane and Boussinesque approximation observing the asymmetry of the poles. Rivière et al. (2012) discuss the potential vorticity perspective on the motion of a mid-latitude winter storm. For a detailed

*Corresponding author. e-mail: annette.mueller@met.fu-berlin.de

Citation: Tellus A: 2020, **72**, 1811535, https://doi.org/10.1080/16000870.2020.1811535

summary of the PV structures see Hoskins and James (2014).

On the convective scale, the PV has only rarely been studied. On this smaller scale, the sinks and the sources of the PV are more or less indispensable. The sources and sinks induced by diabatic processes and friction lead us to analyze the non-conservation of the PV. A fundamental diabatic process is the release of latent heat. It is accompanied by convective cells, and often related to the generation of strong precipitation. Chagnon and Gray (2009), Weijenborg et al. (2015, 2017) and Oertel et al. (2020) consistently show a horizontal PV dipole structure around convective updrafts. So far, the smaller scale PV structure has been analyzed investigating vertical integrated PV anomalies centered at the maximum upwind of a convective cell.

In this context further questions arise, which will be tackled theoretically as well as statistically. How are the PV structures related to the maximal precipitation intensity? Can the horizontal PV dipole be detected and explained as phenomena on the convective scale without taking into account the Coriolis effect as important characteristic of the large scale dynamics? How does the spatial PV structure change during the development of convective cells? It is therefore necessary to analyze the relation of the time evolution of the PV with the time evolution of the precipitation in a statistical setting.

To answer these questions, this work is structured as follows. We will start with Ertel's vorticity theorem as basis for the derivation of the potential vorticity conservation as well as the sources and sinks in Section 2. In Section 3, we will first summarize the classical explanations of the vertical and horizontal PV dipole structure on the synoptic and on the convective scale. There we will show the close relation of the spatial PV structure to the relative vorticity structure in greater detail, where the twisting term of the vorticity equation plays a crucial role. This close relationship results in a novel explanation of the horizontal PV dipole on the convective scale. The occurrence of the horizontal PV dipole for strong convective events will be confirmed statistically by the evaluation of 15 222 precipitation events using the COSMO-REA2 data set, described in Section 5. The variables are divided into different classes of precipitation intensity and evaluated for different time steps. The numerical scheme to identify such extreme events and to evaluate the three-dimensional PV structures and the corresponding variables is outlined in Section 6. In Section 7, the 3D structure of the absolute potential vorticity (Section 7.3) and the 3D structure of the relative potential vorticity without the Coriolis parameter (Section 7.1) confirm the theory, that the development and shape of the horizontal PV dipole structure depend on the Coriolis parameter, being more pronounced in the relative potential vorticity composites. Additionally, the structures of the potential temperature anomaly and the vertical velocity (Sections 7.4 and 7.5) are shown. The results will be discussed and finally summarized in Sections 8 and 9.

2. Theoretical aspects of the potential vorticity (PV)

In 1942, H. Ertel published his pioneering work on the Lagrangian conservation of potential Vorticity (PV) (Ertel, 1942a). Since then, the PV and its conservation law have been frequently used to diagnose and analyze atmospheric motion. Today it can be seen as one of the most fundamental conservation laws in geophysical fluid dynamics. It is an interesting quantity, because it couples vorticity dynamics with thermodynamical processes unifying the information on the distributions of the density, the temperature, and the vorticity field into one scalar. Moreover, its individual conservation is often proposed to be a helpful tool to estimate failings in the numerical weather prediction models (see, e.g. Roulstone and Norbury, 2013).

Ertel derived a seminal vortex theorem as a commutation-relation by introducing the arbitrary field variable ψ. For example, choosing ψ as the local position leads to the Helmholtz vorticity theorems. Thus, Ertel's representation combines all vortex theorems. It also allows the integration of diabatic processes in the equation for the potential vorticity (Ertel, 1942b). On the larger, synoptic scale, the atmosphere is typically considered as an inviscid fluid. Including the mass conservation in the three-dimensional vorticity equation and multiplying this equation by the gradient of a field variable ψ, the resulting equation can be interpreted as the time evolution of the general potential vorticity Π_ψ :

$$\left[\frac{d}{dt}\right]\left[\frac{\boldsymbol{\xi_a}\cdot\nabla}{\rho}\right]\psi-\left[\frac{\boldsymbol{\xi_a}\cdot\nabla}{\rho}\right]\left[\frac{d}{dt}\right]$$
$$\psi=\frac{1}{\rho}\frac{\partial(\psi,p,\nu)}{\partial(x,y,z)},\quad \Pi_\psi=\frac{\boldsymbol{\xi}_a\cdot\nabla\psi}{\rho} \tag{1}$$

(see also Hollmann, 1963). Here, ρ is the density, $\nu=\frac{1}{\rho}$ the specific volume, p the pressure, ψ an arbitrary field variable, and $\boldsymbol{\xi}_a$ denotes the absolute 3D vorticity vector. For viscous fluids, the term $\frac{1}{\rho}(\nabla\times\mathbf{F})\cdot\nabla\psi$ is added on the right hand side of (1), where $\mathbf{F}$ denotes the frictional force. Choosing the potential temperature as field variable:

$$\psi\rightarrow\theta(p,\nu)=T\left(\frac{p_N}{p}\right)^{R_d/c_p}, \tag{2}$$

where the pressure follows from the ideal gas law $p=R\rho T$, and assuming adiabatic flows, the determinant on

the right hand side in (1) vanishes leading to the following individual conservation of the absolute potential vorticity Π_a for adiabatic, inviscid flows:

$$\frac{d\Pi_a}{dt} = 0 \quad \text{with} \quad \Pi_a = \frac{\boldsymbol{\xi}_a \cdot \nabla\theta}{\rho} \ . \tag{3}$$

Further, the relative potential vorticity (PV) without Coriolis parameter will be denoted as Π with the PV-Unit 1 PVU $= 10^6$ K m^{2}kg^{-1}.

Small scale convective processes such as intense precipitation events are related to diabatic heating and to the release of latent heat above the boundary layer. Therefore, individual changes of the temperature ($d\theta/dt = \dot{\theta} \neq 0$) on the convective scale play a crucial role and cannot be neglected on the convective scale. But the diabatic processes lead to changes of the potential vorticity - the PV is not conserved any longer. Taking the diabatic heating and friction into account, the time evolution of the potential vorticity reads as:

$$\frac{d\Pi_a}{dt} = \frac{1}{\rho}(\boldsymbol{\xi}_a \cdot \nabla\dot{\theta} + \nabla \times \mathbf{F} \cdot \nabla\theta) \tag{4}$$

(see Hoskins et al., 2007). While the first summand on the right hand side incorporates diabatic processes such as the latent heat release, the second term contains the frictional force **F**. In this study we will assume diabatic flows, but neglect friction. Under these assumptions the potential vorticity evolution equation is given by:

$$\frac{d\Pi_a}{dt} = \frac{\boldsymbol{\xi}_a \cdot \nabla\dot{\theta}}{\rho} \tag{5}$$

where Π is defined as in (3).

3. Classical explanations of the PV dipole structures

Diabatic heating that accompanies convective events leads to the potential vorticity becoming non-conservative. Sources and sinks of the PV can be observed and PV dipole structures become visible. We will start this section with a summary of the current state of research on the vertical and horizontal PV dipoles. Then, we will analyze the horizontal potential vorticity dipole in more detail regarding the tilting term of the vorticity equation. In Section 7, we will confirm the theoretical results by evaluating cases of intense precipitation events statistically.

The vertical dipole of the non-reduced PV is typically explained by the diabatic heating term $\dot{\theta}$ in the PV evolution equation (5) (see, e.g. Raymond and Jiang, 1990; Pomroy and Thorpe, 2000; Chagnon and Gray, 2009). Consider the diabatic process of developing clouds on the meso-scale and a trajectory of an ascending air parcel in the updraft region. Regarding (5), a PV dipole can only be generated, if the diabatic process contains background vorticity, otherwise the PV evolutional equation would be zero. However, the PV along this ascending air parcel changes, because the condensation processs of water leads to the release of latent heat. The release of latent heat causes a change of the potential temperature with time ($\dot{\theta}>0$). While the air parcel is ascending, the change of the heating rate with height is positive ($\partial\dot{\theta}/\partial z>0$) as well as the absolute vorticity vector. Formulating the equation for the PV evolution (5) componentwise, we obtain for the Lagrangian total time derivative:

$$\begin{aligned}\dot{\Pi}_a &= \frac{1}{\rho}\boldsymbol{\xi}_a \cdot \nabla\dot{\theta} \quad = \frac{1}{\rho}(\xi_{a,x}, \xi_{a,y}, \xi_{a,z}) \cdot \left(\frac{\partial\dot{\theta}}{\partial x}, \frac{\partial\dot{\theta}}{\partial y}, \frac{\partial\dot{\theta}}{\partial z}\right) \\ &= \frac{1}{\rho}\Bigg[\underbrace{\left(\frac{\partial w}{\partial y} - \frac{\partial v}{\partial z}\right)\frac{\partial\dot{\theta}}{\partial x}}_{\text{term 1}} + \underbrace{\left(\frac{\partial u}{\partial z} - \frac{\partial w}{\partial x} + \ell\right)\frac{\partial\dot{\theta}}{\partial y}}_{\text{term 2}} \\ &\quad + \underbrace{\left(\frac{\partial v}{\partial x} - \frac{\partial u}{\partial y} + f\right)\frac{\partial\dot{\theta}}{\partial z}}_{\text{term 3}}\Bigg] \ .\end{aligned} \tag{6}$$

Strong diabatic heating accompanied by background vorticity leads to a dominating term 3 in (6).[1] Due to the heating the PV is positive at the lower troposphere. The PV enlarges until the maximum of the diabatic heating is achieved (see also Raymond and Jiang, 1990) Therefore, a positive temperature gradient in the lower-middle troposphere can be observed. Above the maximum of $\dot{\theta}$, the potential temperature decreases with height, i.e. $\partial\dot{\theta}/\partial z<0$ inducing a negative PV structure. Thus, a vertical PV dipole is generated. The explanation of the vertical dipole especially holds for the larger, synoptic scale, where the Coriolis parameter f influences the atmospheric motion and emphasizes the prevalence of term 3 in (6) that leads to the vertical PV dipole.

The horizontal PV dipole is characteristic for the smaller scale, where the Coriolis force can be neglected. We will show theoretically that on the smaller scale, the PV is strongly related to the relative vorticity. Davies-Jones (1984) analyze the relative vorticity with respect to an inviscid, adiabatic, linear model. He found a relation of the generation of relative vorticity dipoles due to the vertical distortion of the isentropics induced by strong vertical motion. Cammas et al. (1999) relate the generation of the horizontal PV dipole to slanting absolute vorticity vectors, to the latent-heat release, and to a strong vertical wind-shear environment. Studying the evolution of the PV in the convective domain of a mesocyclone, Conzemius and Montgomery (2009) showe a strong relation between the upwind of the individual storm cells and the generation of the relative vorticity vector induced by the tilting mechanism of the horizontal

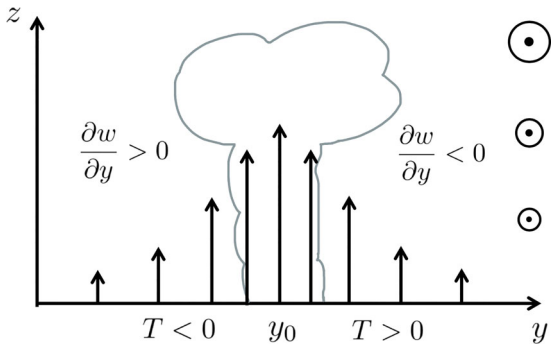

Fig. 1. A sketch of a convective cloud. The black arrows show the updraft.

vorticity. The authors found positive as well as negative small-scale horizontal PV anomalies.

Theoretically, the dipole can be explained by the formula of the individual time evolution of the potential vorticity (6), assuming a strong vertical wind shear of the horizontal wind and a horizontal change of the vertical wind. Furthermore, we assume that the gradient of the horizontal wind changes its sign in the center of the maximum updraft, as sketched in Fig. 1. Then, term 1 and term 2 in (6) increase and induce the relative vorticity in term 3. It follows that term 3 becomes the dominating term in the PV equation. If a horizontal vorticity dipole exist, a horizontal PV dipole will coexist with mirror axis along the direction of propagation of the convective cell.

A further theoretical explanation of the PV dipole on the storm scale was introduced by Chagnon and Gray (2009). The storm scale can be regarded as meso-scale, where the Coriolis parameter cannot be neglected. Therefore, Chagnon and Gray (2009) consider the PV representation based on the linearized Boussinesq equations including the Coriolis parameter f. They derive the angles α and β that describe the angles between the vertical PV dipole and the horizontally tilted PV dipole. In their approach, the Coriolis parameter is an important parameter for their theoretical explanation of the PV dipole on the meso-scale. A vertical dipole can be assumed for barotropic conditions and in the case of a baroclinic atmosphere, the increased angles lead to a horizontal PV dipole. Following Chagnon and Gray (2009), the angles depend on the strength of the vertical wind shear of the horizontal wind and the spatial extent of the heating rate. They are given by

$$\alpha = \arctan\left(\frac{\frac{\partial \mathbf{v}_h}{\partial z}}{f}\right) \quad \text{and} \quad \beta = \arctan\left(\frac{f\sigma_x^2}{\frac{\partial \mathbf{v}_h}{\partial z}\sigma_y^2}\right) \tag{7}$$

where σ_x and σ_y denote the length scale of the Gauss-distributed heating rates in x- and y-direction,[2] see the sketch of the PV dipole in Fig. 2. Therefore, it is confirmed theoretically that a strong vertical wind shear of the horizontal wind is an important ingredient for the generation of the horizontal dipole. This result is statistically corroborated by Weijenborg et al. (2015). Moreover, Chagnon and Gray (2009) and Weijenborg et al. (2015) show that the strength and the direction of the PV dipoles can be related to the vertical wind shear. In particular, regarding (6) the heating terms $\frac{\partial \dot{\theta}}{\partial x}$ and $\frac{\partial \dot{\theta}}{\partial y}$ can be seen as source-terms for the time evolution of the potential vorticity. Moreover, regarding (7), a variation of the Gaussian distributed heating rates σ_x and σ_y leads to a deformation of the horizontal PV dipole structure. The vertical or horizontal arrangement of the PV dipole is determined by the ratio of the horizontal expansion of the heating and the vertical wind shear of the horizontal wind. While the Coriolis parameter is a parameter that determines the arrangement of the PV dipole on the meso-scale, see equation (7), on the smaller, convective scale the Coriolis effect does not influence the atmospheric motion, as will be explained in the next section.

4. A theoretical explanation of the horizontal dipole on the convective scale

The following analysis of the horizontal PV dipole for strong convective processes is based on the twisting term of the vorticity equation. Here, we will focus on the convective scale, where the Coriolis parameter does not contribute to the equations of motion. We start with the equation for the vertical component of the vorticity for incompressible flows:

$$\frac{d\zeta}{dt} = \mathbf{k}\cdot\frac{d\boldsymbol{\xi}}{dt} = \mathbf{k}\cdot(\boldsymbol{\xi}\cdot\nabla\mathbf{v}) = \underbrace{-\zeta\nabla_h\cdot\mathbf{v}_h}_{D} \underbrace{-\mathbf{k}\cdot\left(\nabla_h w\times\frac{\partial \mathbf{v}_h}{\partial z}\right)}_{T_z}, \tag{8}$$

where D denotes the horizontal divergence term, T_z the so-called twisting term and $\mathbf{k}$ is the unit vector in z-direction. The twisting term can further be formulated as:

$$T_z = \mathbf{k}\cdot\left(\nabla_h w\times\frac{\partial \mathbf{v}_h}{\partial z}\right) = \frac{\partial w}{\partial x}\frac{\partial v}{\partial z} - \frac{\partial w}{\partial y}\frac{\partial u}{\partial z}\,. \tag{9}$$

The gradient $\partial\mathbf{v}_h/\partial z$ denotes the change of the horizontal wind with height, which reflects the baroclinicity on the synoptic scale. The expression $\nabla_h w$ denotes the horizontal change of the vertical wind, which becomes in particular important for the embedded convective updrafts on the smaller scale. Combining both terms, the twisting term T_z couples the dynamics on the convective scale with the dynamics on the synoptic scale.

As initial state we consider a convective process with strong wind shear, as sketched in Fig. 1. The large horizontal gradient of the vertical velocity and the strong

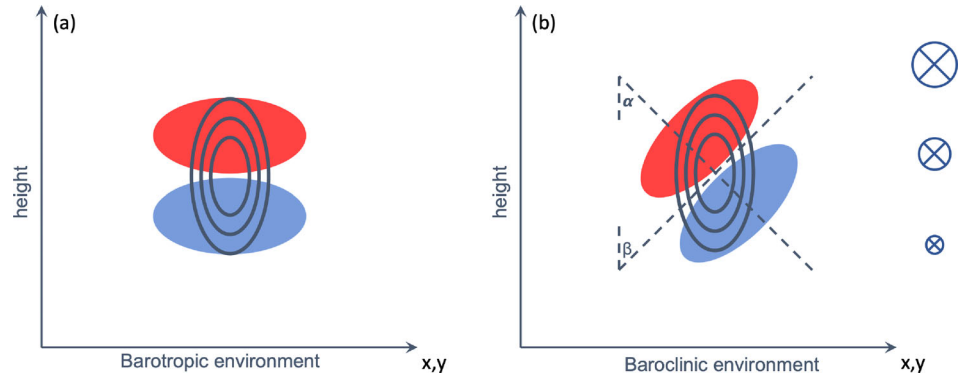

Fig. 2. (a) Shows a sketch of the vertical PV dipole caused by heating for a barotropic environment. (b) Indicates the tilt of the dipole caused by the horizontal gradient of the vertical velocity and by the vertical change of the horizontal velocity. The red region indicates the positive pole and the blue region shows the positive pole. The figures are adapted from Chagnon and Gray (2009).

vertical gradient of the horizontal velocity lead to a dominating twisting term T_z in (8). The twisting term describes the change of the rotational angle of the vortex tube from a horizontally rotating vortex to a tilted vortex that rotates about a vertical axis. This tilting process is only possible, if the horizontal gradient of the vertical velocity and the horizontal component of the vorticity vector are sufficiently large. Furthermore, both terms must not be perpendicular. In case they are perpendicular, the twisting term (9) would vanish (see also Pichler, 1997). Jones (1995) emphasizes the importance of the vertically sheared environmental flow for a generation of a horizontal PV dipole. We notice that the thermodynamical activation ($\nabla\dot{\theta} \gg 0$) is directly related to the dynamical activation of the twisting term.

As an example to illustrate the tilting mechanism, consider a strong convective updraft at y_0 that decreases along the y-axis in both directions, i.e. the updraft decreases for smaller as well as for larger y-values, as sketched in Fig. 1. Moreover, we assume an increasing wind with height $\left(\frac{\partial v_h}{\partial z} > 0\right)$ that blows eastwards along the x-axis. Then, the horizontal gradient of the vertical wind is positive for $y<y_0$ and negative for $y>y_0$, as illustrated in Fig. 1. It follows that the sign of the twisting term (9) is positive for $y>y_0$ and negative for $y<y_0$:

$$T_z = \begin{cases} >0 & \text{for } y>y_0 \\ <0 & \text{for } y<y_0 \end{cases} . \tag{10}$$

We recall that the idealized vorticity equation (8) can be written as sum of the divergence and the twisting term. Restricting the vorticity equation to the twisting term, the sign of the individual temporal change of the vorticity changes in y_0 conversely to the sign of the twisting term:

$$\left.\frac{d\zeta}{dt}\right|_{T_z} = \begin{cases} <0 & \text{for } y>y_0 \\ >0 & \text{for } y<y_0 \end{cases} . \tag{11}$$

Thus, in the case that the divergence term can be neglected, the horizontal dipole structure of the vorticity can be explained. In Sections 7.1 and 7.5, we will show that at the height, where the dipole of the relative PV is most pronounced, the vertical velocity is maximal. Using the continuity equation shows that the divergence term D can indeed be neglected for strong convective processes.

Moreover, in the following we will show that in case of strong convective updrafts, the vorticity equation is directly related to the PV equation. Therefore, a significant dipole structure can also be observed in the 3D composites of the PV. To show this relation, we start with the Eulerian decomposition of the potential temperature:

$$\frac{d\theta}{dt} = \frac{\partial\theta}{\partial t} + \mathbf{v}_h \cdot \nabla_h\theta + w\frac{\partial\theta}{\partial z} . \tag{12}$$

We assume that the vertical component of the diabatic heating gradient is greater than the horizontal heating rates, i.e. $\nabla\dot{\theta} \gg 0$ with $\frac{\partial\dot{\theta}}{\partial z} \gg \frac{\partial\dot{\theta}}{\partial x}$ and $\frac{\partial\dot{\theta}}{\partial z} \gg \frac{\partial\dot{\theta}}{\partial y}$, which is confirmed in the composites of the potential temperature anomaly in Fig. 3. This assumption leads to the following relation:

$$\dot{\theta} \sim w\frac{\partial\theta}{\partial z} . \tag{13}$$

Inserting the Brunt Väisälä frequency $N_z^2 = \frac{g}{\theta}\frac{\partial\theta}{\partial z}$ leads to:

$$\dot{\theta} = \left(\frac{\theta}{g}N_z^2\right)w \tag{14}$$

Therefore, for strong convective processes, the vertical velocity is proportional to the diabatic heating term up to a measure of hydrostatic stability:

$$\dot{\theta} \sim w . \tag{15}$$

We remark that Haynes and McIntyre (1987) came to the same proportionality regarding the p-system and the stability parameter σ. This relation is clearly visible in the composites of the potential temperature anomaly and the vertical velocity shown in Fig. 4 and in Fig. 3. Both composites will be discussed more in detail in Section 7. Inserting the relation of the diabatic heating to the vertical velocity into the equation for the PV, the PV equation becomes proportional to the vorticity equation (8):

$$\dot{\theta} \sim w \quad \Rightarrow \quad \frac{d\Pi}{dt} = \boldsymbol{\xi} \cdot \nabla \dot{\theta} \sim \boldsymbol{\xi} \cdot \nabla w = \frac{d\zeta}{dt} \ . \tag{16}$$

This means that in this approximation the time evolution of the potential vorticity is determined by the divergence term D and the twisting term T_z of the vorticity equation.

$$\frac{d\Pi}{dt} \sim \frac{d\zeta}{dt} = -D - T_z \ . \tag{17}$$

Moreover, it follows that the vortex motion depends on the wind and can be expressed without a thermodynamical quantity. Therefore, the source term induces a vorticity equation for an ideal fluid. Thus, there is a possible relationship to conservation properties of numerical schemes through the energy-vorticity as introduced for the shallow water model by Sommer and Névir (2009).

The proportionality (17) and its derivation also holds for the potential vorticity and the absolute vorticity with Coriolis parameter, as still as the vertical component of the diabatic heating gradient is greater than the horizontal heating rates. In Section 7, the statistical analysis will show that the horizontal PV dipole structure on the convective scale is especially distinct without Coriolis parameter. This can be explained by theoretical considerations. Moreover, similar to Pedlosky (2013), Klein (2010) or Müller et al. (2018) a scale analysis could show in which order the Coriolis parameter can be neglected. Thus, we use the proportionality of the relative vorticity and the relative PV without Coriolis parameter.

Under the condition of strong convection, we can expect similar spatial structures for the (relative) vorticity and (relative) potential vorticity. We have shown that the horizontal PV dipole can be explained by the twisting term of the vorticity equation, generated by diabatic heating and by a strong horizontal gradient of the vertical velocity accompanied by a strong vertical wind shear of the horizontal wind. The horizontal gradient of the vertical velocity and the vertical gradient of the horizontal wind are equally important. Thus, the dynamics should be considered in a three-dimensional isotropic space, which is characteristic for the convective scale. The composites in Sections 7.1 and 7.5 will show that at the height, where the dipole of the relative PV is most pronounced, the vertical velocity is maximal. Using the continuity equation, this leads to a vanishing divergence term. Thus, regarding (17) without considering the Coriolis parameter, the 3D twisting term plays a crucial role for convective processes. This theory can further be confirmed by a multiscale aymptotic analysis as proposed by Hittmeir and Klein (2018).

To underline the importance of the dipole structure arising from the above discussed tilting process, we note that the tilting process is characterized by a dipole of a further important conserved quantity, the helicity. The dipole structure of the helicity for strong convective events is discussed e.g. by Lilly (1986), Klemp (1987), Markowski and Richardson (2011) and Weijenborg et al. (2015). The helicity density h is defined as

$$h = \frac{1}{2} \mathbf{v} \cdot \boldsymbol{\xi} \ . \tag{18}$$

Consider the setup from our last example, sketched in Fig. 1, where the storm moves eastwards, i.e. in x-direction, with constant velocity and centered at y_0. Then, the helicity density h of this example reduces to:

$$h = \frac{1}{2} u \cdot \frac{\partial w}{\partial y} \ , \quad \text{where} \quad h = \begin{cases} <0 & \text{for } y > y_0 \\ >0 & \text{for } y < y_0 \end{cases} \ . \tag{19}$$

Therefore, the helicity density changes its sign in the center of the updraft y_0 in Fig. 1. The helicity density has negative values northwards ($y<y_0$) of the storm and positive values southwards ($y>y_0$) of the storm.

To summarize, the vertical wind shear of the horizontal wind on the synoptic scale and the embedded horizontal shear of the vertical wind on the smaller convective scale, are conditions for the generation of strong convective activity with heavy precipitation. These conditions lead to the tilt of the vorticity and a horizontal dipole structure of the relative vorticity is generated. Then, the here shown proportionality of the vorticity to the potential vorticity explains the potential vorticity dipole. In the following sections, the COSMO-REA2 data set will be applied to confirm statistically the horizontal dipole structures of the vorticity and the PV during strong precipitation events.

5. Data

To analyze the PV structure with respect to strong convective events and to corroborate and extend the results of Weijenborg et al. (2015) and Chagnon and Gray (2009), the COSMO-REA2 reanalysis data set is used. The COSMO model is a non-hydrostatic, numerical weather prediction model based on the thermo-hydrodynamical equations of motions for compressible fluids (Doms and Baldauf, 2018). The horizontal resolution of the COSMO-REA2 data is 0.018° (about 2 km) covering the

domain of Germany. Vertically, the model has 50 layers following the orography, where the geometric height above sea level ranges between 10 m and 22 km. The data set allows for a suitable study of the PV structure during precipitation processes on the convective scale. Bollmeyer et al. (2015) show that compared to other reanalysis data sets such as COSMO-REA6 or ERA-Interim the COSMO-REA2 data set has a better correlation to the observed and modelled precipitation, because of the incorporated latent heat nudging. For more details of the models see Wahl et al. (2017), Dee et al. (2011) and Doms and Baldauf (2018).

In the following, the precipitation events of the months June, July and August during the time period 2007–2012 are analyzed. The 3D wind, the temperature, the pressure and the total precipitation of the COSMO-REA2 data set with a time resolution of one hour is used to calculate the density, the potential temperature, the vorticity and the potential vorticity. To neglect boundary effects, 60 grid points to the west, to the north, and to the east are excluded. Furthermore, to the south, the Alps are excluded to neglect the orographic effects. The evaluated domain is shown in Fig. 5. The number of precipitation events is equally distributed into different classes of precipitation intensity, see Table 1. As lower bound of class the intensity of 5 mm/h was chosen, which is moderate precipitation after the classification of the German Weather Service (DWD, 2019). The evaluated cases of precipitation events sum up to a total number of 15 222 cases. We will focus on the structures of potential vorticity with and without Coriolis parameter, the relative vorticity, the vertical velocity and the potential temperature anomaly of the most intense precipitation events.

6. Methods

To study the PV structure during strong convective processes, first, the precipitation events are identified and classified into classes A-D. In this study, we will focus on the values in class D with a precipitation intensity greater than 29 mm/h, which are identified as extreme values. For a better evaluation of the PV, all variables defining the potential vorticity are calculated and rotated such that all precipitation cells move into the same direction. This procedure leads to an analysis in the Eulerian view. In the following, the steps are presented in detail, for a summary see Fig. 6.

1. All grid points with precipitation are identified and equally distributed into the four classes A (precipitation intensity 4.0–5.1 mm/h), B (intensity 10–10.6 mm/h), C (20–24 mm/h) and D ($\geq$29 mm/h), see also Table 1. The relative frequencies of the events and the corresponding intensity classes are shown in Fig. 7.
2. 11×11 grid boxes around the grid boxes with precipitation intensities of classes A-D are considered. In this domain, the grid boxes of the minimum and maximum precipitation intensity are located. Finally, larger grids of size 27×27 (about 54 km) are centered at the precipitation maximum to achieve continuous structures. For each grid box in this domain the precipitation intensity, the date and the time are saved.
3. For the domains of the previous step, the same information is saved for four further time steps (one and two hours before, and one and two hours after the precipitation maximum is reached). In this way, the precipitation intensity, the date and the time is saved for five time steps.
4. It is checked that the precipitation maximum is the middle time step.
5. In each case the following variables are saved for all five time steps: the 3D wind vector components, the temperature, the pressure and the precipitation. Additionally, these data are saved for two further time steps before the five selected days, see Table 2.

Table 1. The intensity classes with respect to the precipitation intensity.

Class	A	B	C	D
Intensity in mm/h	4.9–5.1	10–10.6	20–24	$\geq$29
Percentil	97.15–97.35	99.40–99.48	99.90–99.95	$\geq$ 99.97
Number of events	3975	3665	3797	3785

Table 2. The variables given at the selected points of time. The maximum precipitation intensity is at t_{max}.

Variables: Time:	$t_{max}-4h$	$t_{max}-3h$	$t_{max}-2h$	$t_{max}-1h$	t_{max}	$t_{max}+1h$	$t_{max}+2h$
Total precip.			x	x	**x**	x	x
u,v,w,T,p	x	x	x	x	**x**	x	x

6. The 3D vorticity $\boldsymbol{\xi}$, the potential temperature θ and the potential vorticity Π are calculated. Thereby, the constants $R_d = 287.05 Jkg^{-1}K^{-1}, c_p = 1005.7 Jkg^{-1}K^{-1}, p_N = 1000 hPa$ are defined and the density is calculated in terms of the ideal gas law $\rho = pR_d^{-1}T^{-1}$.
7. Finally, all data fields are rotated so that all precipitation events are aligned propagating towards a common direction of propagation. This leads to a suitable representation to analyze the temporal change of the spatial structures of the variables. First, for each precipitation event and at each point of time the mean horizontal wind direction between 500 and 600 hPa is determined. Then, the angle of rotation is given by the angle between the mean horizontal wind direction and the x-axis. Finally, the fields are rotated about this angle such that all precipitation events move towards the x-direction.

The above steps lead to 336 composites (4 intensity classes $\times$ 14 variables $\times$ 6 time steps ($t_{max}-3h$ to $t_{max}+2h$). The data at the time $t_{max}-4h$, i.e. 4 hours before the precipitation maximum is reached, is used for the significance test. Usually, the lifetime of convective cells is about 10 minutes to 1 hour. Therefore, the distribution of the grid points at time $t_{max}-4h$ can be seen as mean state before the precipitation event. Thus, it is an appropriate choice for the reference time for the significance test.

7. 3D composites of the PV and related variables

In this section, the composites of the potential vorticity and the related variables during extreme precipitation events ($\geq$29 mm/h) are shown. Regarding these composites in Figs. 3, 4 and 8–10 the different perspectives on the 3D visualizations are marked by the small letters a)-d), where a) is the topview onto the x-y-plane, b) and c) show the x-z and the y-z-planes, and d) is the full 3D plot with (x, y, z) coordinates. In each figure, the units of x, y, z are kilometers. To compare the structures of the variables, all fields were rotated such that they move into the x-direction, as explained in the previous section. Thereby, at time $t_{max}-1h$ the maximum precipitation is located in the origin of the $x-y$-plane ($x = y = 0$).

We will start with the 3D composites of the relative PV (without Coriolis force), where a significant dipole structure can be observed. Additionally, we will show the 3D composites of the relative vorticity, the absolute PV, the potential temperature anomaly and the composites of the vertical velocity. In each Figs. 3, 4 and 8–10, the first column shows the different perspectives of the variable one hour before the accumulated precipitation maximum ($t_{max}-1h$) and the second column shows the different perspectives of the variable at the time of maximum precipitation intensity (t_{max}).

7.1. Composites of the relative potential vorticity

As shown in Fig. 11, the structure can be recognized particularly well in the composites of the relative potential vorticity, where the Coriolis force is neglected. Fig. 8 shows the significant ($\alpha = 0.05$) relative potential vorticity composites of the precipitation intensity class D. The black contours are the isolines of the mean precipitation in intervals of 2 mm/h, starting at 3.0 mm/h. We recall that the precipitation domain is rotated such that all precipitation events progress in x-direction.

At time $t_{max}-1h$ the dipole structure of the relative potential vorticity is centered slightly behind the precipitation maximum. While the positive pole extends from the ground up to a height of 8 km, the negative pole ranges vertically from about 3 to 8 km. The domination of the positive pole is also reflected in the values in PV units that range between -1.1 and $+2.1$.

At time t_{max}, at which the precipitation reaches its maximum, the positive pole expands both horizontally and vertically. Now, the positive and the horizontal poles have almost the same horizontal extent. At this time, the clearly visible dipole structure has moved higher and is stretched in the direction of propagation. Moreover, the values in PV units of both poles have increased up to -1.7 and $+2.4$.

At the following points of time, $t_{max}+1h$ and $t_{max}+2h$, the relative potential vorticity dipole structures weaken fast, so that they are hardly recognizable. Moreover, at the time $t_{max}-4h, t_{max}-3h$ and $t_{max}-2h$ the relative potential vorticity structure cannot, or only rarely be identified. For the additional composites of the relative potential vorticity at classes of less intense precipitation (class A-C) see the supplementary material.

To summarize, a significant horizontal dipole of the relative PV close to the precipitation maximum can be observed. The dipole structure is characterized by a distinct positive pole and a negative pole, which has a smaller vertical extent. The absolute values as well as the vertical extent of both poles reach their maximum during the moment of maximal precipitation intensity.

7.2. Composites of the relative vorticity

The relative vorticity dominates the structure of the relative potential vorticity. In Section 4, we have shown theoretically that for strong convective updrafts, the temporal evolution of the relative potential vorticity is proportional to the temporal evolution of the vorticity. This theory is corroborated by the 3D composites of the

relative vorticity in Fig. 9. A significant horizontal dipole similar to the dipole of the relative potential vorticity in Fig. 8 can be recognized.

At $t_{max}-1h$, the dipole of the relative vorticity is placed slightly behind the precipitation maximum. While vertically the positive pole reaches from the ground up to about 8 km, the negative pole reaches from a geometrical height of 3 km to 7.3 km. The relative vorticity dipole is centered at the same height as the dipole of the relative potential vorticity. The maximal value of the positive relative vorticity pole ($3.7 \cdot 10^{-4} s^{-1}$) is more than twice as large as the maximal value of the negative pole ($-1.7 \cdot 10^{-4} s^{-1}$). We call a process, that is mainly related to the 3D wind and its derivations, dynamical, and we call it thermodynamical, if it is mainly determined by temperature and pressure anomalies. Then, considering this dipole structure as a vortex split, it can be assumed that the basic mechanism of the split is not related to a thermodynamical process, but to a process that can be explained as a purely dynamical.

At t_{max}, the negative relative vorticity pole has enlarged as well vertically as horizontally. Therefore, a distinct dipole structure can be observed. While the maximal values of the positive pole do not change during the previously hour, the smallest negative value decreases from $-1.7 \cdot 10^{-4} s^{-1}$ to $-2.5 \cdot 10^{-4} s^{-1}$. At this time of maximal precipitation, the positive pole is extended radially near the ground, and in the middle troposphere the dipole has moved in the direction of propagation. We compare the relative vorticity in Fig. 9 with the relative potential vorticity in Fig. 8. This comparison shows that the radial extension of the positive pole near the ground as well as the horizontal extension near the boundary layer, are more distinct in the composites of the relative vorticity than in the composites of the relative potential vorticity.

For the apparent influence of the relative vorticity on the relative PV in the precipitation intensity classes A-C and for further time steps in the intensity class D, see the supplementary material.

7.3. Composites of the absolute potential vorticity

The composites of the absolute potential vorticity including the Coriolis parameter of the intensity class D at the times $t_{max}-1h$ and t_{max} are shown in Fig. 10.

The absolute PV composites at time $t_{max}-1h$ are shown in the first column, where the positive pole is strongly pronounced. Vertically, the positive absolute PV pole has the same extent as the relative vorticity and the relative potential vorticity. It ranges from the ground to a height of about 8 km. Furthermore, the dipole is centered at the same height as the dipoles of the the relative vorticity and the relative PV composites, too. The negative pole of the absolute PV is only rarely visible. This is also reflected in the values that have a minimum of 0.4 PVU. The maximal absolute PV value in the troposphere, one hour before the precipitation maximum, is 2.7 PVU. Horizontally, the absolute vorticity dipole is centered slightly behind the maximal precipitation contour and extends in opposite direction of the propagation.

At the time of maximal precipitation t_{max} the main dipole structure is located at positive x-values. Especially in the middle-upper troposphere the positive pole extends in the direction of propagation. At this time, the negative pole becomes more visible and the minimum decreases to -1.0 PVU. The positive pole increases to a maximum of 3.2 PVU. During the next hour $t_{max}+1h$, the PV structure almost vanishes, as shown in the appendix.

While a significant dipole structure of the relative PV without Coriolis parameter could be observed, the positive pole of the absolute PV with Coriolis force is much more distinct than the negative pole. We can conclude that the Coriolis effect supresses the development of a distinct dipole structure in the absolute PV growth rate.

7.4. Anomaly-composites of the potential temperature

The composites of the potential temperature anomalies of intensity class D are shown in Fig. 3. We recall that the figures a) in the first row are from the top view onto the $x-y$-plane. In the first column the potential temperature anomalies are represented at the time $t_{max}-1h$ and the second column shows the corresponding plots for the time t_{max}, at which the precipitation maximum is reached. For the calculation of the anomaly, the potential temperature field at time $t_{max}-4h$ was chosen as reference field, because the lifetime of small scale, convective processes is usually much shorter than 4 hours.

The red isosurfaces show the positive anomalies that indicate the heating of the air masses. The blue isosurfaces represent the negative anomalies that reflect the cooling of the air. The additional black contours in Fig. 3 indicate the mean accumulated precipitation of the next hour, starting at 3.0 mm/h in intervals of 2 mm/h.

At time $t_{max}-1h$ two distinct anomalies can be recognized. Vertically, the negative potential temperature anomaly reaches from the ground up to about 3 km. The positive anomaly reaches from 2.8 km to the tropopause. The maximal positive anomaly is located in a height of 4.8 km, where the previously discussed dipole structures of the relative vorticity and the relative and absolute potential vorticity were found. Horizontally, the positive pole is centered at the precipitation maximum, and the center of the negative anomaly is located behind the precipitation maximum in the quadrant of negative x values

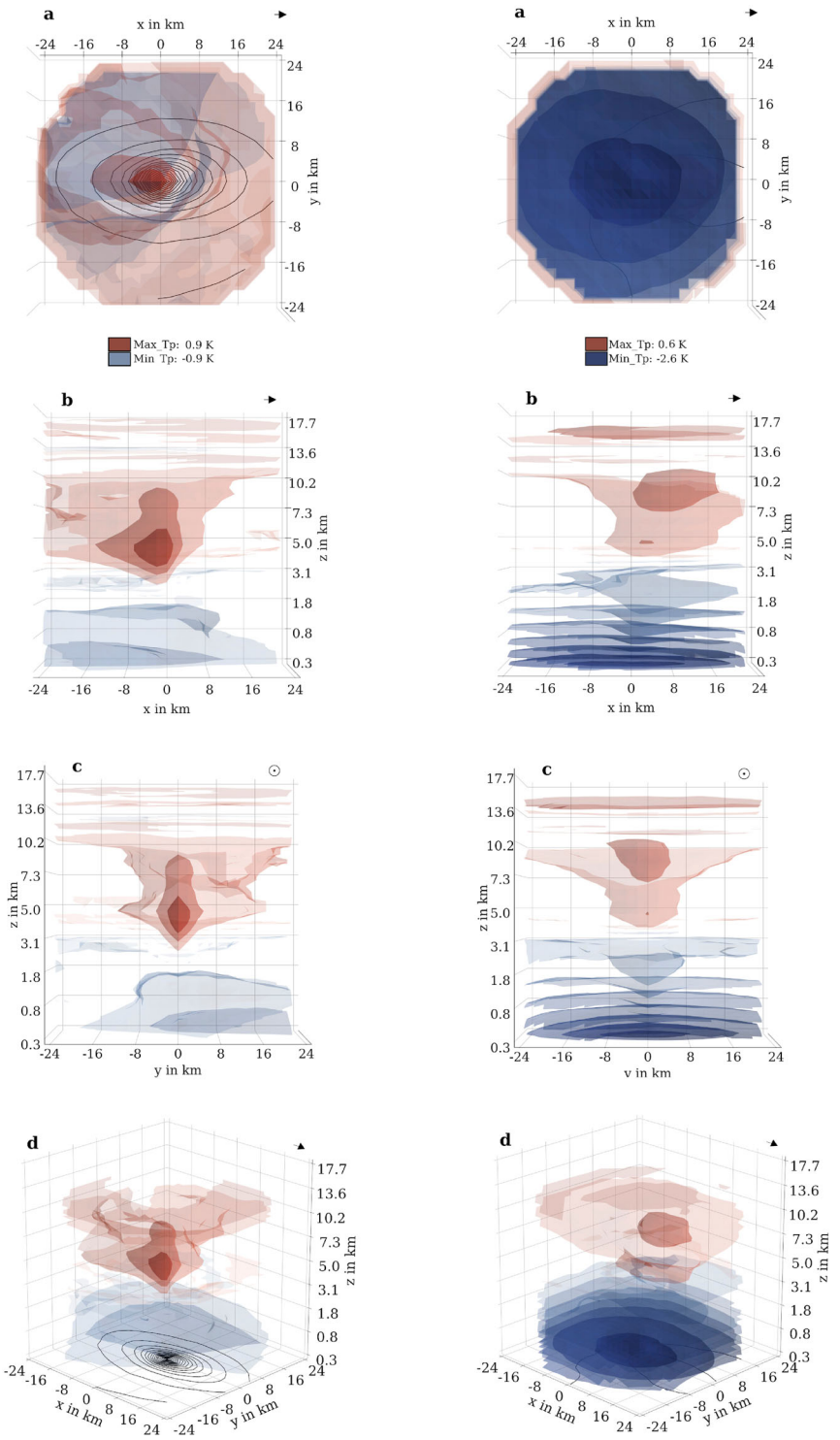

Fig. 3. The anomaly composites of the potential temperature for intensity class D for the time $t_{max}-1h$ (first column) and $t_{max}-$ (second column) are shown. The rows are the different perspectives a, b, c and d. Max_{Tp} and Min_{Tp} denote the maximal and minimal value of the potential temperature anomaly in the troposphere. The red/blue isosurfaces mark the positive/negative values, where the isosurfaces become darker as the absolute values increase. The black contours show the precipitation sum of the next hour in 2 mm/h intervals.

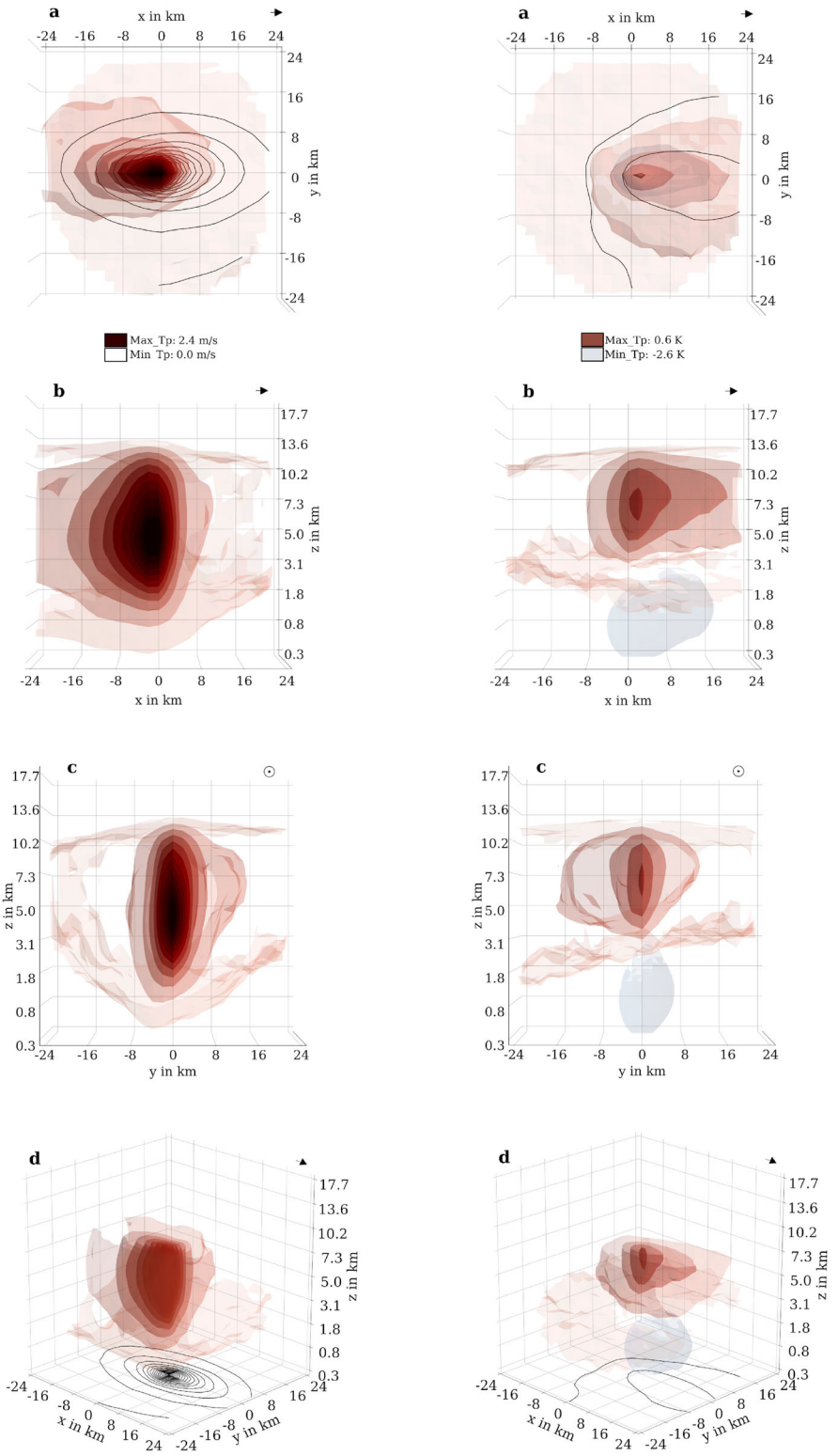

Fig. 4. The composites of the vertical velocity for intensity class D for the time steps $t_{max}-1h$ (first column) and t_{max} (second column) are illustrated, where the rows are the different perspectives a, b, c and d. Max_{Tp} and Min_{Tp} denote the maximal and minimal vertical velocity in the troposphere. The red/blue isosurfaces mark the positive/negative values, where the isosurfaces become darker as the absolute values increase. The black contours show the precipitation sum of the next hour in 2 mm/h intervals.

and positive y values. Physically, the negative anomaly, which has its minimum at 0.9 K, describes the cooling of the air. The positive anomaly shows the additional warming of up to 0.9 K

At time t_{max} the negative anomalies reach −2.6 K and the maximal positive anomaly is weakened to 0.6 K. The whole structure is shifted upwards. Now, the maximal positive anomaly lies about 5 kilometers higher than one hour earlier.

Consider the process of diabatic heating in an unstable atmosphere. Warm air at the ground ascends towards the upper cold air. The process of convection has a stabilizing effect and leads to the generation of clouds. This is reflected in the composites of the potential temperature anomaly: In the geometric height of the latent heat release, a positive potential temperature anomaly can be recognized in the upper troposphere. In the lower troposphere on the other side, a negative temperature anomaly is generated.

7.5. Composites of the vertical velocity

Deep moist convection is always related to strong vertical updrafts. The composites of the significant vertical velocity are shown in Fig. 4. The left column in Fig. 4 shows the vertical velocity composites at the time $t_{max}-1h$, where the upwind is clearly visible, especially from the perspectives b) and c) that show the x-z and the y-z-planes. The vertical velocity reaches a maximum of 2.4 m/s and the core-isosurfaces with values larger than 0.3 m/s are located shortly behind the precipitation maximum. The vertical expansion of the vertical velocity ranges from the lower boundary layer to the tropopause. The vertical location and extension is in agreement with the position and the height of the positive potential temperature anomaly pattern. Moreover, the core of the vertical velocity lies between the negative and positive pole of the relative potential vorticity (see Fig. 9). Horizontally, similar to the potential temperature anomaly in the middle troposphere in Fig. 3, the isosurfaces of the vertical velocity extends in opposite direction of the storm propagation.

At the time t_{max}, the maximum of the vertical velocity decreases to 0.9 m/s. Furthermore, the vertical extent is reduced and the position is vertically shifted about 2 km upwards. In comparison to the precipitation field, the region of the upwind still lies behind the center of the maximal precipitation, with respect to the direction of

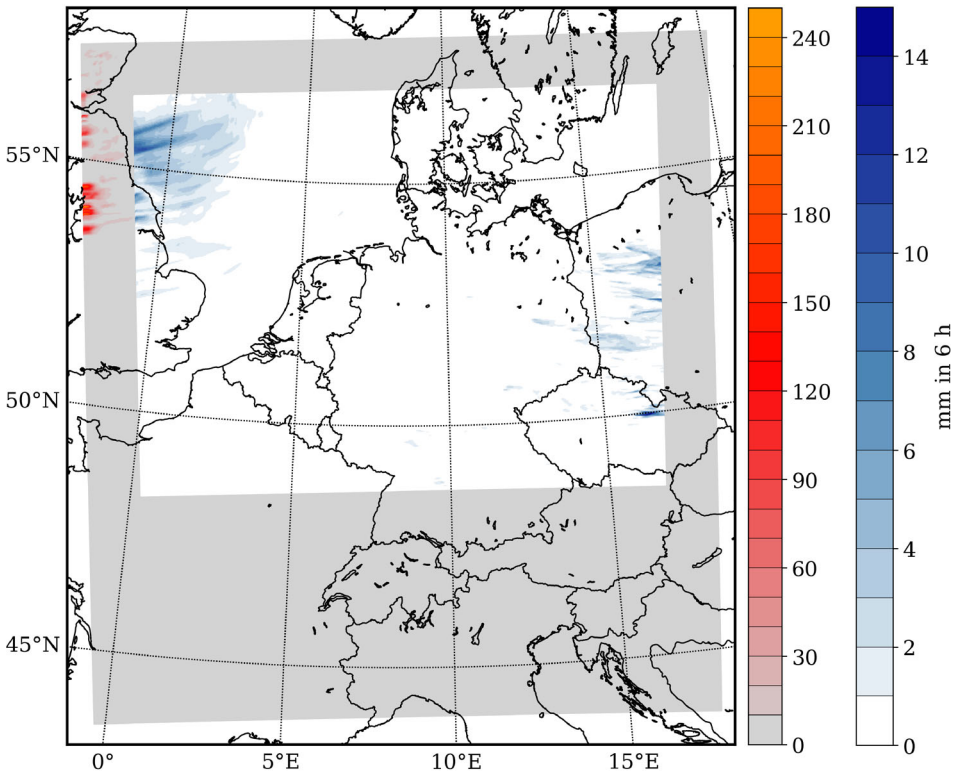

Fig. 5. The domain of the COSMO-REA2 data set (gray box) and the data domain analyzed here (inner white box). The blue colorbar shows the precipitation (6 h-sum) from 29.06.2007 at 0:00 UTC with respect to the inner domain. The red colorbar shows the precipitation inside the gray box.

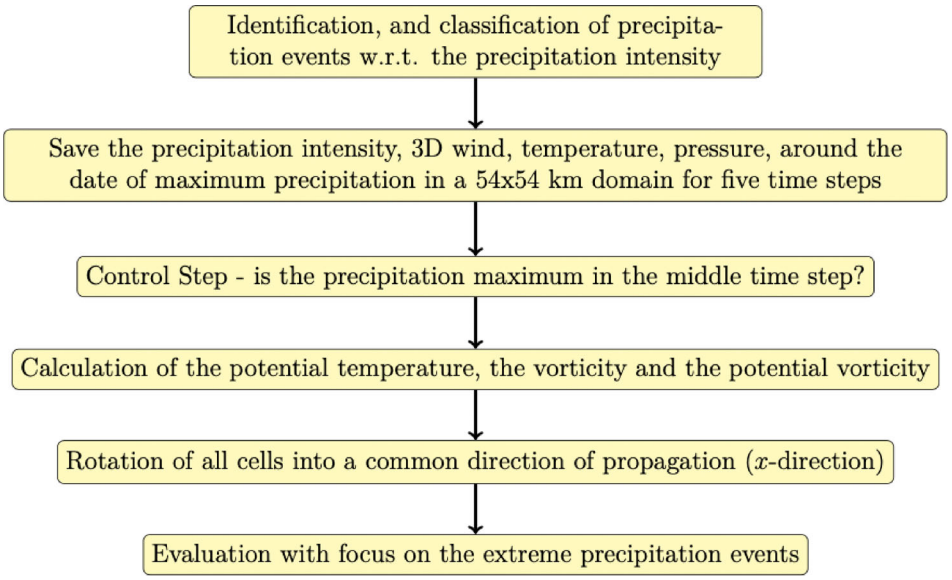

Fig. 6. The steps to identify and calculate the 3D composites of the PV and the related variables during intense precipitation events are summarized. The categories of the precipitation intensities are listed in Table 1.

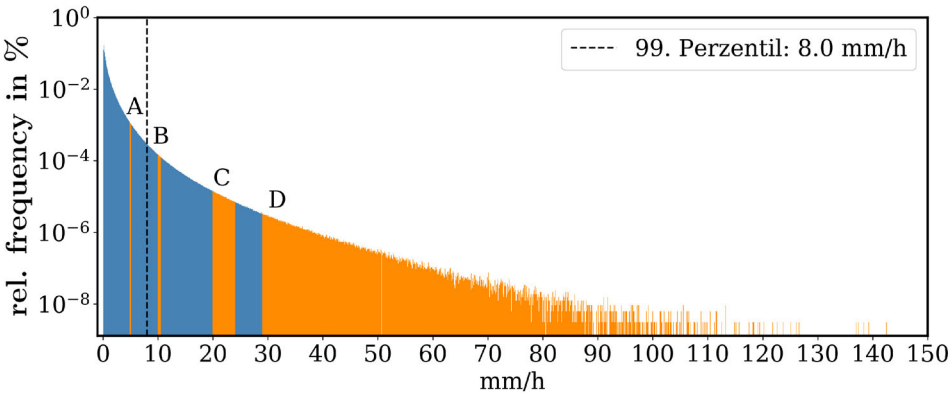

Fig. 7. Relative frequency (logarithmic profile) of a precipitation intensity larger than 0.1 mm/h (blue) and the percentiles of the intensity classes of Table 1 (orange). The black dashed lines shows the 99. percentile.

propagation. The structure slightly spreads horizontally into the direction of the cell propagation.

The vertical height of the updraft coincides with the height of the dipole of the relative potential vorticity. The strong relation of the precipitation intensity and the updraft can be recognized particularly well from the top views in the first row.

At the time of the maximal precipitation t_{max}, shown in the second column in Fig. 4, downdrafts below the upwind maxima can be observed with a minimum of −0.3 m/s.

8. Discussion

Three-dimensional composites are used to analyze the structure of the PV with and without Coriolis parameter and the relative vorticity statistically, during extreme precipitation events for different time steps. This topic has been studied earlier in the framework of two case studies by Weijenborg et al. (2015), who discuss the PV structure on two days, one day with convection along a cold front, and a second day, where local severe convection was observed. We investigated the relation of the PV structure to precipitation statistically from the Eulerian view and

with respect to the maximal precipitation intensity, whereas Weijenborg et al. (2015) identified the storm cells in terms of strong vertical velocities inside the upwind area to evaluate 2D composites of PV anomalies from the Lagrangian perspective.

The first question we asked in the introduction was how the PV structure is related to the maximal precipitation intensity. To answer this question we focused on the class of extreme precipitation events with precipitation intensities larger than 29 mm/h. Thereby, all precipitation cells are rotated such that they have a common direction of propagation. The three-dimensional composites of the relative PV without Coriolis parameter show a distinct horizontal PV dipole at the time of maximal precipitation intensity, see Fig. 8. Furthermore, the coexistence of a significant horizontal dipole of the relative vorticity located spatially as well as temporally close to the precipitation maximum can be observed in Fig. 9. The dipole structures of the relative PV and the relative vorticity consist of a positive pole to the right and a negative pole to the left of the moving precipitation cell, which is in accordance with the results of the case study of Weijenborg et al. (2015).

The dipole structures of the relative PV without Coriolis parameter are more visible than the pattern of the PV with Coriolis parameter. Considering the potential vorticity with Coriolis parameter, the vertical extent of the positive pole is much larger than the vertical extent of the negative pole, which is only rarely visible, see Fig. 10. Thus, the relative PV dipole pattern is more symmetric than the absolute PV dipole pattern. In the context of a case study using COSMO simulations in a 2.2 km grid Oertel et al. (2020) show an asymmetric dipole centered at the precipitation maximum with a dominating negative PV pole. Thereby, the authors considered the PV with Coriolis parameter to represent the dynamics on the meso-scale. The asymmetry of the poles of the absolute vorticity is also shown in the studies of Viúdez (2010) and Cammas et al. (1999).

The question arise, if the dipole structure can be explained by the dynamics on the convective scale alone, or if an interaction of the convective scale with the synoptic scale is required. To analyze the relevance of the larger scale Coriolis effect the maxima and minima of the potential vorticity with and without Coriolis parameter are determined and summarized in Table 3. These PV values are listed for the hourly time steps $t_{max}-3h$ to $t_{max}+2h$. Spatially, the PV values from the ground up to a hight of 8.5 km are considered. These values confirm that the dipoles of the PV with and without Coriolis parameter are most distinct at the time of maximal precipitation. At this time both potential vorticity expressions reach the maximal positive and the minimal negative values. The relative PV ranges between −1.7 PVU and 2.4 PVU and the absolute PV has values from −1.0 PVU to 3.2 PVU. Regarding the absolute PV, only during the hour before the maximal precipitation and during the hour of maximal precipitation, the absolute PV has a negative pole. Therefore, compared to the absolute PV, the dipole structure of the relative PV is more symmetric, which shows the existence of the PV dipole on the convective scale. Furthermore, we note that the here calculated absolute potential vorticity differs from the absolute PV for the quasi-geostrophic model, which is given by the sum of the relative potential vorticity and the Coriolis term. Thus, we may conclude that the gradient of the potential temperature has an effect on the absolute PV, especially in the case of strong convective processes.

The similarity of distinct dipoles of the vorticity and the PV at the time of maximum precipitation corroborates the strong relation of the potential vorticity with the relative vorticity, that we derived analytically in Section 4. The horizontal dipole structures of both variables can be explained as follows. Strong convective activity is characterized by a strong vertical wind shear of the horizontal wind and by an increasing wind with height, as sketched in Fig. 1. Both gradients have a meaningful influence on the PV dipole structures. Non-zero gradients of the geostrophic wind on the synoptic scale ($\frac{\partial \mathbf{v}_{h,g}}{\partial z} \approx \frac{\partial \mathbf{v}_h}{\partial z} \neq 0$) reflect the baroclinic effects on the larger scale. The horizontal gradient of the vertical velocity ($\frac{\partial w}{\partial x}, \frac{\partial w}{\partial y}$) reflects great variations of the small scale convective activity. The importance of the horizontal gradient of the vertical wind for the stability of the dipole is also shown by Lilly (1986), who take the helicity (19) into account. As stronger the horizontal gradient of the vertical wind, as larger the helicity, and large helicity values are characteristic for long living vortex dipoles (see e.g. Lilly, 1986). While the direct comparison of the minima and maxima values of the PV with and without Coriolis parameter in the previous paragraph showed the existence of the dipole on the convective scale, the interaction of the convective and the synoptic scale provides a necessary condition for the persistence and the intensity of the dipole structures.

We have shown that the interaction of the large scale vertical gradient of the horizontal wind with the small scale horizontal gradient of the vertical wind determine the twisting term T_z (9) in the vorticity equation and finally explain the dipole of the absolute and relative potential vorticity: if the gradients in the twisting term of the vorticity equation become large, the twisting term in the vorticity equation dominates. Comparing Fig. 8 with Fig. 4 we recognize that at the height, where dipole of the relative PV is most pronounced, the vertical velocity is maximal. Applying the continuity equation shows that

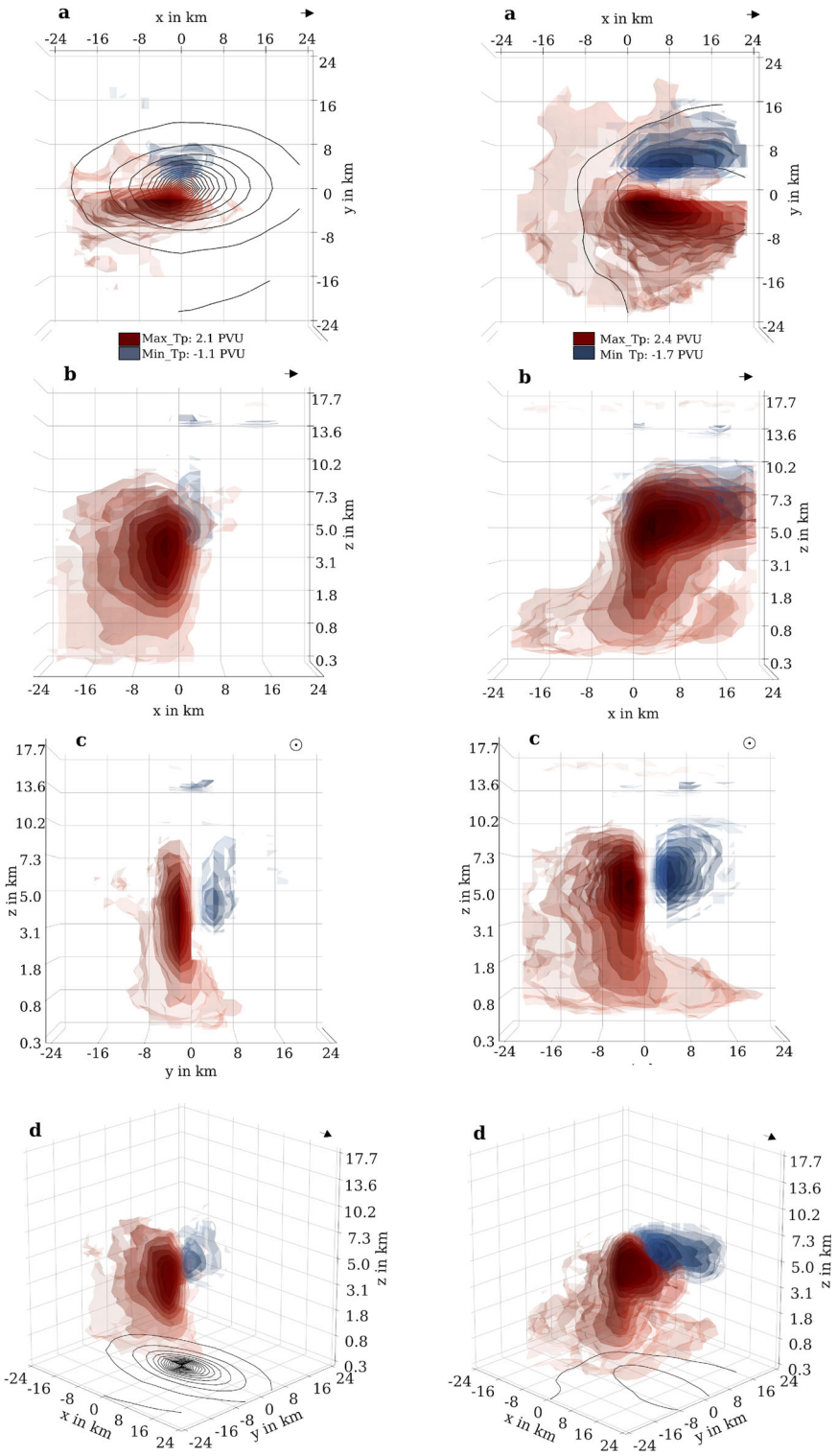

Fig. 8. Composites of the relative PV for intensity class D for the time one hour before the maximal precipitation intensity ($t_{max}-1h$; first column) and at the time of maximal precipitation intensity t_{max} (second column). The rows are the different perspectives a, b, c and d. Max_{Tp} and Min_{Tp} indicate the maximal and minimal value of the relative PV in the troposphere, where only values from the ground up to a height of 8.5 km were taken into account. Positive values of the variables are indicated by red isosurfaces, where the surfaces become darker as the values increase. Negative values are marked by blue isosurfaces, where the darkness increases, when the absolute values become higher. The black contours show the precipitation sum of the next hour in 2 mm/h intervals.

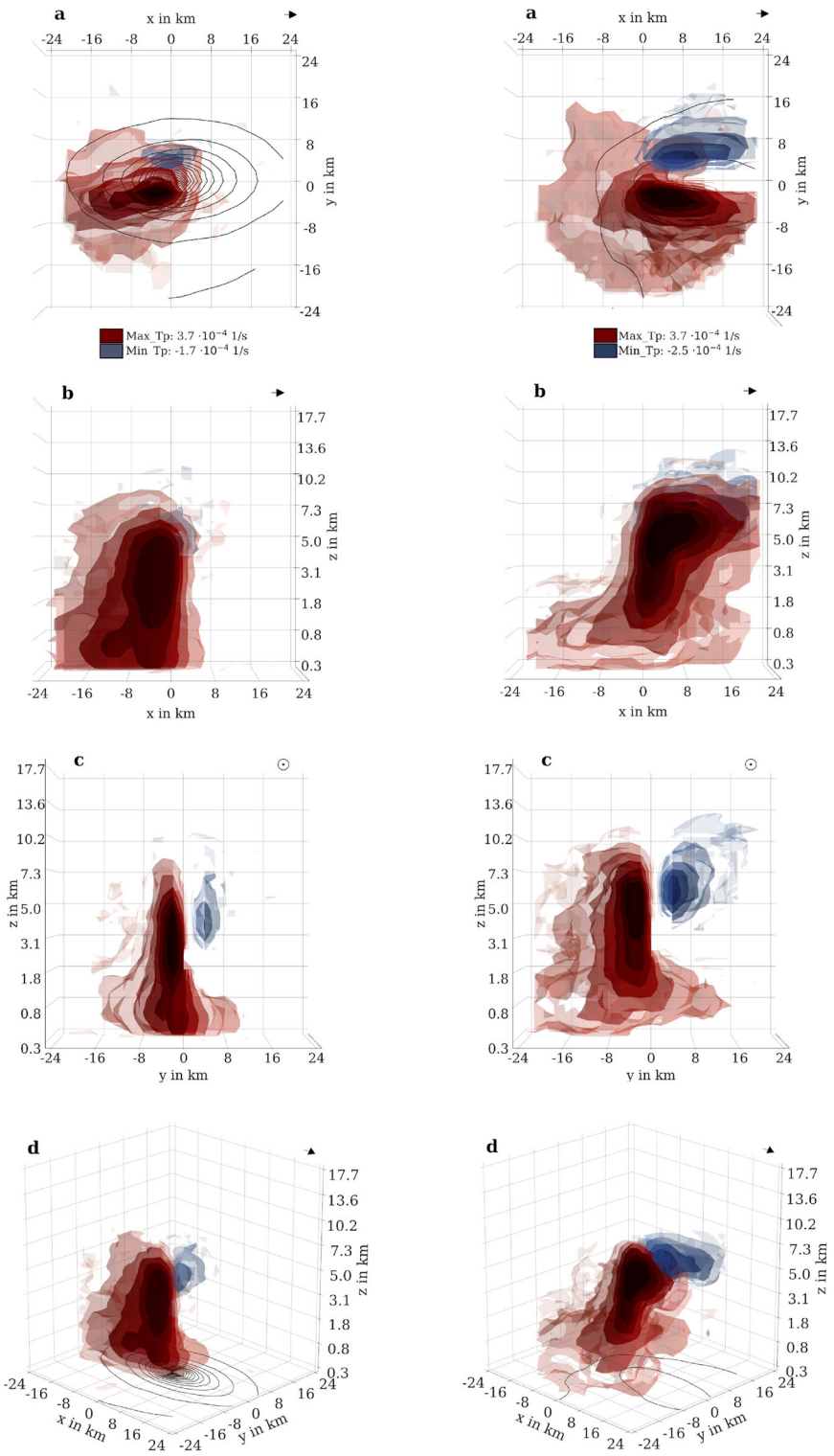

Fig. 9. The first column shows the composites of the relative vorticity ζ for intensity class D at the time $t_{max}-1h$ and the second columns shows the relative vorticity at the time t_{max}. The rows are the different perspectives a, b, c and d. Max_{Tp} and Min_{Tp} denote the maximal and minimal value of the vorticity in the troposphere. Red/blue isosurfaces mark the positive/negative values, where the isosurfaces become darker as the absolute values increase. The black contours show the precipitation sum of the next hour in 2 mm/h intervals.

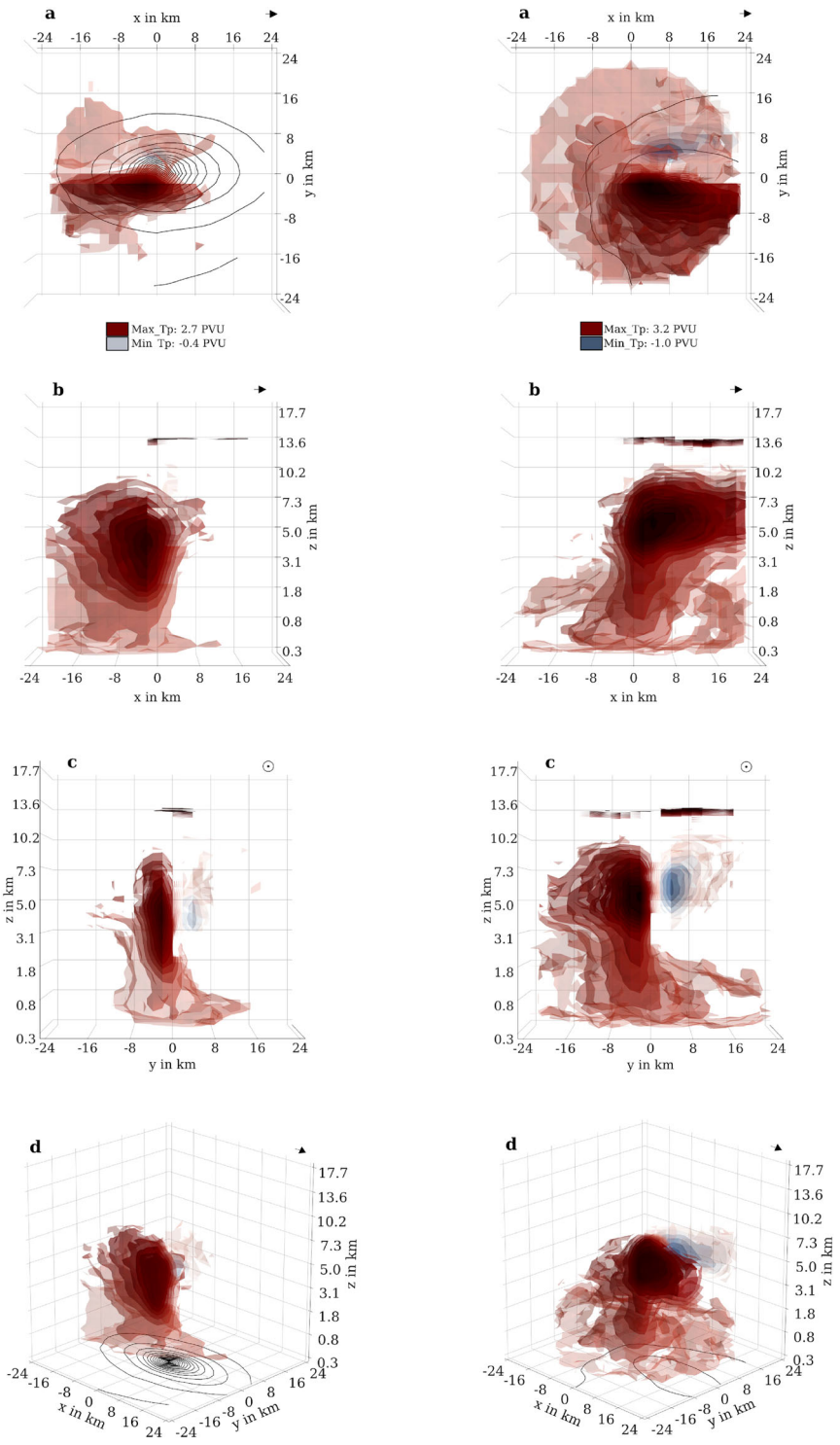

Fig. 10. The composites of the absolute PV for intensity class D for the time steps $t_{max}-1h$ (first column) and t_{max} (second column) are illustrated, where the rows are the different perspectives a, b, c and d. Here, Max_{Tp} and Min_{Tp} denote the maximal and minimal value of the absolute PV in the troposphere and as in the previous figures, the red/blue isosurfaces mark the positive/negative values, where the isosurfaces become darker as the absolute values increase. The black contours show the precipitation sum of the next hour in 2 mm/h intervals.

Table 3. The maximal and minimal values of the potential vorticity with and without Coriolis parameter from the ground up to a height of 8.5 km.

Variables: Time:	$t_{max}-3h$	$t_{max}-2h$	$t_{max}-1h$	t_{max}	$t_{max}+1h$	$t_{max}+2h$
Maximum relative PV	0.3	0.4	2.1	2.4	0.5	0.3
Maximum absolute PV	0.9	1.0	2.7	3.2	1.2	1.0
Minimum relative PV	−0.1	−0.2	−1.1	−1.7	−0.3	−0.2
Minimum absolute PV	0.2	0.2	−0.4	−1.0	0.2	0.2

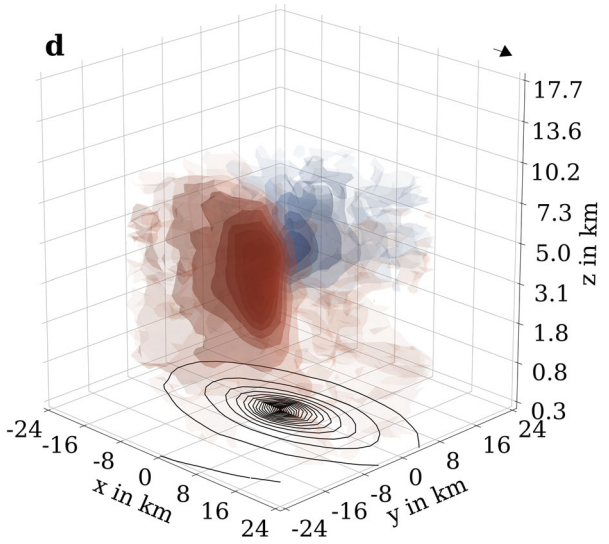

Fig. 11. The relative PV composites of 3785 extreme precipitation events for the time step ($t_{max}-1h$) is shown clearly indicating the horizontal dipole structure.

the divergence D term is zero. Thus, for strong convective processes we obtain the following relation:

$$\frac{d\Pi}{dt} \sim \frac{d\zeta}{dt} = -D - T_z \approx -T_z \ . \tag{20}$$

The dominating twisting term leads to the vortex tilt and finally to the horizontal vortex dipole.

Furthermore, assuming strong convection, we show that the vertical velocity is proportional to the diabatic heating term (see also Haynes and McIntyre, 1987). The composites of the vertical velocity and the potential temperature anomalies in Fig. 4 and in Fig. 3 corroborate this theoretical result. This proportionality finally leads to the proportionality of the vorticity and PV equations of motions (16), (20) and explains the coexistence of the horizontal dipoles in the PV and the vorticity field.

In contrast to the here observed horizontal dipole on the small scale, a vertical dipole can be observed on the large scale, see e.g. Raymond and Jiang (1990) or Chagnon and Gray (2009). So far, the conditions for the generation of a horizontal PV dipole were investigated theoretically by Chagnon and Gray (2009). The authors considered the storm scale as meso-scale, where the Coriolis parameter plays an important role, and confirmed their theory of the PV dipole by a numerical case study.

In the introduction we asked the question, if the horizontal PV dipole can be detected and explained as phenomena on the convective scale without taking the influence of the Coriolis effect into account. The comparison of the PV structures with and without Coriolis parameter show that the Coriolis effect prevents the development of a strong horizontal dipole. Thus, the horizontal dipole seems to be an important characteristic on the convective scale directly explained by the dynamics of the convective scale. Therefore, we propose the use of the relative PV for further investigations restricted on the convective scale.

For a deeper insight into the PV structure, the composites of the variables defining the PV mathematically are also shown. The potential temperature anomaly and the vertical velocity, see Figs. 3 and 4, are seemingly related to the PV: The center of the positive potential temperature anomaly has the same local position (horizontal and vertical) as the center of the horizontal dipole of the relative PV. This common feature underlines the relation of the PV to the release of latent heat. Furthermore, the local position of the vertical velocity coincides locally with the center of the horizontal dipole of the relative PV.

The third question we asked in the introduction was about the change of the PV structure during the development of convective cells. We found that the the structure of all analyzed variables is clearest during the time of maximal precipitation, see Figs. 8 and 10 and the supplementary material. We note that the temporal resolution of one hour is relatively coarse. For a more precise study of the pattern of variables during the development, a smaller temporal resolution is desirable.

9. Conclusion

The 3D composites of the potential vorticity (PV) with and without Coriolis parameter show a horizontal PV dipole structure on the convective scale during extreme

precipitation events. The patterns of the PV with and without Coriolis parameter, as well as the patterns of the vorticity and of the vertical velocity are all spatially and temporally correlated with intense precipitation. The statistical composites confirm our theoretical explanation of the horiztontal PV dipole in Section 2, where we show the proportionality of the vorticity equation and the PV equation of motion in the case of strong convection. While in previous studies PV *anomalies* where investigated (Weijenborg et al., 2015, 2017; Oertel et al., 2020), we concentrated on the PV itself, where no reference state needs to be chosen. To generate the 3D composites all precipitation cells are rotated into a common direction of propagation.

On the convective scale, where the Coriolis force can be neglected, a horizontal PV dipole is a characteristic of strong convective motion. We have explained theoretically and investigated statistically that for strong convective events the 3D composites of the relative PV without Coriolis force and the relative vorticity, are characterized by coexisting dipole structures. The horizontal dipoles, with poles located to the right and left of the moving storm, were in particular reflected in the relative potential vorticity field and the relative vorticity field.

From the perspective of scale interaction, the generation of the horizontal PV dipole can be seen as the interplay of the vertical shear of the horizontal wind on the synoptic scale with the horizontal shear of the vertical wind on the convective scale. Theoretically, this can be explained by the twisting term in the vorticity equation and the proportionality of the time evolution of the PV and the vorticity.

Summarizing, we explained theoretically and corroborated statistically the horizontal PV dipole for extreme precipitation events on the convective scale. A three-dimensional isotropy is generated, if the horizontal and vertical wind shear have the same order of magnitude. This isotropy, characteristic for heavy precipitation events, identifies the relative potential vorticity as a useful quantity to diagnose and study atmospheric phenomena and processes on the convective scale.

Acknowledgments

The authors thank the unknown reviewer for helpful comments and suggestions. We also thank Tracy Kiszler for careful reading the manuscript and Martin Rudolph for reproducing Fig. 2. The authors thank the University of Bonn and the German Weather Service (DWD) for providing the COSMO-REA 2 data set and the Deutsche Forschungsgemeinschaft for their support within the framework of CRC 1114 'Scaling Cascades in Complex Systems', project A01. The authors acknowledge support by the Open Access Publication Fund of the Freie Universität Berlin.

Supplemental data

Supplemental data for this article can be accessed here

Notes

1 Recall the notation for the wind vector components $\mathbf{v} = (u, v, w)$, and the Coriolis parameter vector $(0, \ell, f)$ with $\ell = 2\Omega\cos(\varphi)$ and $f = 2\Omega\sin(\varphi)$.

2 Chagnon and Gray (2009) assume a Gaussian heating profile of the form $B = c\exp\left[-\left(\frac{x-x_0}{2\sigma_x^2} + \frac{z-z_0}{2\sigma_z^2}\right)\right]$ with the location of the centre of the heating (x_0, y_0), the heating length-scales in the cross-frontal and vertical directions σ_x and σ_z, and c denotes the constant maximum amplitude of the heating rate B.

References

Bollmeyer, C., Keller, J., Ohlwein, C., Wahl, S., Crewell, S. and co-authors. 2015. Towards a high-resolution regional reanalysis for the european cordex domain. *Q. J. R. Meteorol. Soc.* **141**, 1–15. doi:10.1002/qj.2486

Cammas, J.-P., Pouponneau, B., Desroziers, G., Santurette, P., Joly, A. and co-authors. 1999. Fastex iop17 cyclone: Introductory synoptic study with field data. *Q. J. R. Meteorol. Soc.* **125**, 3393–3414. doi:10.1002/qj.49712556114

Chagnon, J. M. and Gray, S. L. 2009. Horizontal potential vorticity dipoles on the convective storm scale. *Q. J. R. Meteorol. Soc.* **135**, 1392–1408. doi:10.1002/qj.468

Conzemius, R. J. and Montgomery, M. T. 2009. *Clarification on the Generation of Absolute and Potential Vorticity in Mesoscale Convective Vortices*. Technical Report, Dept. of Meteorology, NAVAL Postgraduate School Monterey, CA.

Davies-Jones, R. 1984. Streamwise vorticity: The origin of updraft rotation in supercell storms. *J. Atmos. Sci.* **41**, 2991–3006. doi:10.1175/1520-0469(1984)041<2991:SVTOOU>2.0.CO;2

Davis, C. A. 1992. Piecewise potential vorticity inversion. *J. Atmos. Sci.* **49**, 1397–1411. doi:10.1175/1520-0469(1992)049<1397:PPVI>2.0.CO;2

Dee, D. P., Uppala, S. M., Simmons, A., Berrisford, P., Poli, P. and co-authors. 2011. The era-interim reanalysis: Configuration and performance of the data assimilation system. *Q. J. R. Meteorol. Soc.* **137**, 553–597. doi:10.1002/qj.828

Doms, G. and Baldauf, M. 2018. *A Description of the Nonhydrostatic Regional Cosmo Model. Part I: Dynamics and Numerics*. Technical Report, Deutscher Wetterdienst.

DWD. 2019. Wetterlexikon. Online at: https://www.dwd.de/DE/service/lexikon/Functions/glossar.html?lv2=101812&lv3=101906.

Ertel, H. 1942a. Ein neuer hydrodynamischer Wirbelsatz. *Sonderdruck Aus Der Meteorologischen Z* **8**, 277–281.

Ertel, H. 1942b. On hydrodynamic eddy theorems. *Physikalische Zeitschrift* **43**, 526–529.

Haynes, P. H. and McIntyre, M. E. 1987. On the evolution of vorticity and potential vorticity in the presence of diabatic heating and frictional or other forces. *J. Atmos. Sci.* **44**, 828–841. doi:10.1175/1520-0469(1987)044<0828:OTEOVA>2.0.CO;2

Hittmeir, S. and Klein, R. 2018. Asymptotics for moist deep convection I: Refined scalings and self-sustaining updrafts. *Theor. Comput. Fluid Dyn.* **32**, 137–164. doi:10.1007/s00162-017-0443-z

Hollmann, G. 1963. Ein vollständiges System hydrodynamischer Erhaltungssätze. *Arch. Met. Geoph. Biokl. A* **14**, 1–13. doi:10.1007/BF02247751

Hoskins, B. J. and James, I. N. 2014. *Fluid Dynamics of the Mid-Latitude Atmosphere*. Oxford, UK: John Wiley & Sons.

Hoskins, B. J., McIntyre, M. E. and Robertson, A. W. 2007. On the use and significance of isentropic potential vorticity maps. *Q. J. R. Meteorol. Soc.* **111**, 877–946. doi:10.1002/qj.49711147002

Jones, S. C. 1995. The evolution of vortices in vertical shear. I: Initially barotropic vortices. *Q. J. R. Meteorol. Soc.* **121**, 821–851. doi:10.1002/qj.49712152406

Klein, R. 2010. Scale-dependent models for atmospheric flows. *Annu. Rev. Fluid Mech.* **42**, 249–274. doi:10.1146/annurev-fluid-121108-145537

Klemp, J. B. 1987. Dynamics of tornadic thunderstorms. *Annu. Rev. Fluid Mech.* **19**, 369–402. doi:10.1146/annurev.fl.19.010187.002101

Lilly, D. K. 1986. The structure, energetics and propagation of rotating convective storms. Part II: Helicity and storm stabilization. *J. Atmos. Sci.* **43**, 126–140. doi:10.1175/1520-0469(1986)043<0126:TSEAPO>2.0.CO;2

Markowski, P. and Richardson, Y. 2011. *Mesoscale Meteorology in Midlatitudes*, Vol. 2. Oxford, UK: John Wiley & Sons.

Müller, A., Névir, P. and Klein, R. 2018. Scale dependent analytical investigation of the dynamic state index concerning the quasi-geostrophic theory. *Math. Clim. Weather Forecast* **4**, 1–22. doi:10.1515/mcwf-2018-0001

Oertel, A., Boettcher, M., Joos, H., Sprenger, M. and Wernli, H. 2020. Potential vorticity structure of embedded convection in a warm conveyor belt and its relevance for the large-scale dynamics. *Weather Clim. Dynam.* **1**, 127–153. doi:10.5194/wcd-1-127-2020

Pedlosky, J. 2013. *Geophysical Fluid Dynamics*. New York: Springer Science & Business Media.

Persson, P. O. G. 1995. Simulations of the potential vorticity structure and budget of fronts 87 iop8. *Q. J. R. Meteorol. Soc.* **121**, 1041–1081. doi:10.1002/qj.49712152506

Pichler, H. 1997. *Dynamik Der Atmosphäre*. Berlin: Spektrum akademischer Verlag.

Plant, R., Craig, G. C. and Gray, S. 2003. On a threefold classification of extratropical cyclogenesis. *Q. J. R. Meteorol. Soc.* **129**, 2989–3012. doi:10.1256/qj.02.174

Pomroy, H. R. and Thorpe, A. J. 2000. The evolution and dynamical role of reduced upper-tropospheric potential vorticity in intensive observing period one of fastex. *Mon. Wea. Rev.* **128**, 1817–1834. doi:10.1175/1520-0493(2000)128<1817:TEADRO>2.0.CO;2

Raymond, D. and Jiang, H. 1990. A theory for long-lived mesoscale convective systems. *J. Atmos. Sci.* **47**, 3067–3077. doi:10.1175/1520-0469(1990)047<3067:ATFLLM>2.0.CO;2

Rivière, G., Arbogast, P., Lapeyre, G. and Maynard, K. 2012. A potential vorticity perspective on the motion of a mid-latitude winter storm. *Geophys. Res. Lett.* **39**, L12808. doi:10.1029/2012GL052440

Roulstone, I. and Norbury, J. 2013. *Invisible in the Storm: The Role of Mathematics in Understanding Weather*. Princeton: Princeton University Press.

Sommer, M. and Névir, P. 2009. A conservative scheme for the shallow-water system on a staggered geodesic grid based on a nambu representation. *Q. J. R. Meteorol. Soc.* **135**, 485–494. doi:10.1002/qj.368

Thorpe, A. and Emanuel, K. 1985. Frontogenesis in the presence of small stability to slantwise convection. *J. Atmos. Sci.* **42**, 1809–1824. doi:10.1175/1520-0469(1985)042<1809:FITPOS>2.0.CO;2

Viúdez, Á. 2010. Vertical splitting of vortices in geophysical dipoles. *J. Phys. Oceanogr.* **40**, 2170–2179. doi:10.1175/2010JPO4418.1

Wahl, S., Bollmeyer, C., Crewell, S., Figura, C., Friederichs, P. and co-authors. 2017. A novel convective-scale regional reanalysis cosmo-rea2: Improving the representation of precipitation. *Metz.* **26**, 345–361. doi:10.1127/metz/2017/0824

Weijenborg, C., Friederichs, P. and Hense, A. 2015. Organisation of potential vorticity on the mesoscale during deep moist convection. *Tellus A* **67**, 25705. doi:10.3402/tellusa.v67.25705

Weijenborg, C., Chagnon, J., Friederichs, P., Gray, S. and Hense, A. 2017. Coherent evolution of potential vorticity anomalies associated with deep moist convection. *Q. J. R. Meteorol. Soc.* **143**, 1254–1267. doi:10.1002/qj.3000